Annals of Biomedical Engineering, Vol. 33, No. 3, March 2005 (© 2005) pp. 402–412
DOI: 10.1007/s10439-005-1743-9

Derivation of Centers and Axes of Rotation for Wrist and Fingers in a Hand Kinematic Model: Methods and Reliability Results

P. CERVERI,[1,2] N. LOPOMO,[1] A. PEDOTTI,[1] and G. FERRIGNO[1]

[1]Bioengineering Department, Politecnico di Milano, Piazza Leonardo da Vinci, Milano, Italy; and [2]BTS Bioengineering, via Inverigo 2-20151 Milano, Italy

(Received 12 March 2004; accepted 7 October 2004)

Abstract—In the field of 3D reconstruction of human motion from video, model-based techniques have been proposed to increase the estimation accuracy and the degree of automation. The feasibility of this approach is strictly connected with the adopted biomechanical model. Particularly, the representation of the kinematic chain and the assessment of the corresponding parameters play a relevant role for the success of the motion assessment. In this paper, the focus is on the determination of the kinematic parameters of a general hand skeleton model using surface measurements. A novel method that integrates nonrigid sphere fitting and evolutionary optimization is proposed to estimate the centers and the functional axes of rotation of the skeletal joints. The reliability of the technique is tested using real movement data and simulated motions with known ground truth 3D measurement noise and different ranges of motion (RoM). With respect to standard nonrigid sphere fitting techniques, the proposed method performs 10–50% better in the best condition (very low noise and wide RoM) and over 100% better with physiological artifacts and RoM. Repeatability in the range of a couple of millimeters, on the localization of the centers of rotation, and in the range of one degree, on the axis directions is obtained from real data experiments.

Keywords—Hand kinematical model, Rotation centers, Functional axes, Surface markers.

INTRODUCTION

In recent years, significant efforts have been devoted to hand modeling and gesture analysis with the aim of linking finger kinematics to functional ability for biomechanical and clinical assessment.[3–5,11,16,17,20,25,28] Equivalently, considerable research has focused on the problem of capturing articulated finger pose for symbol understanding and command coding in the domains of interhuman communication and human–computer interaction.[23,28] In particular, motion reconstruction techniques have provided the ability to estimate in vivo the 3D motion of finger joints from video-based surface measurements in real-time.[9,10,21,30] In such an approach, the 3D position of physical markers, attached to palpable bony landmarks on the hand, is measured by motion capture systems during articulated hand movements and the kinematic variables of the underlying skeletal structure are computed through a suitable mapping.[18,27] This implies both a kinematic hand model, defined through a hierarchical chain constituted of mechanical joints corresponding to real articulations, and procedures to compute the joint centers (CoR) and axes of rotation (AoR). In general, the identification of the CoRs and AoRs guarantees more accurate description of underlying bone kinematics as well as recognition of possible kinematic modification caused by pathological conditions.[4] It is important to understand that there are no methods readily available for the computation of CoR and AoR of the finger joints from hand articulated movements.

Zhang *et al*.[30] developed an analytical method to derive the CoR from 21 markers during flexion-extension movements. While the presented results appears valuable, the involved optimization strategy was asserted to be computationally nontrivial. In addition, effects of soft tissue artifacts and small range of motion (RoM), which were shown significantly affect the estimated kinematic variables derived from marker motion data,[1,6,22] were not explored. Moreover, the variability of the results on the position of the markers at the finger surface was not investigated. General purpose procedures, based on rigid and nonrigid sphere fitting, were proposed[12,13] for the determination of the averaged CoR and AoR of the lower limb joints but their feasibility to the case of hand model was not assessed. In particular, such methods were recognized to be particularly sensitive to measurement noise and motion artifacts in radial direction when reduced ranges of motion are involved.[19]

In this paper, we present the development of a new method for the calibration of kinematic characteristics of hand skeleton model utilizing motion data of surface markers acquired during controlled articulated hand and finger movements. The performance of this method is compared

Address correspondence to Pietro Cerveri, Dipartimento di Bioingegneria, Politecnico di Milano, Piazza Leonardo da Vinci 32, 20133 Milano, Italy. Electronic-mail: cerveri@biomed.polimi.it

with that of another algorithm proposed in the literature.[12] The kernel of the method rests on nonrigid sphere fitting integrated within an evolutionary optimization algorithm[7] to minimize the variance of the marker distances from the corresponding rotation center or rotation axis. Pure rotational movements of the markers around the corresponding rotation axis or center, the main requirement of all sphere fitting-based methods, are obtained from articulated finger motions by hierarchically decoupling the movements defined in the distal coordinate system from that in the proximal coordinate system. The reliability of the method is evaluated through simulated and real hand motions.

METHODS

Hand Skeleton Model and Marker Protocol

The hand skeleton consists of eight carpal bones, five metacarpal bones and 14 phalanges [see Fig. 1(a)]. Apart from the thumb that has two phalanges, each finger divides into proximal, middle, and distal phalanges. In order to represent the hand skeleton into a kinematic model we used a hierarchical structure of rigidly connected joints, each having one or two rotational degrees of freedom (DoF). While the eight bones of the carpus articulate finely with each other producing small deformation, the representation into a single rigid segment is a consistent approximation.[5]

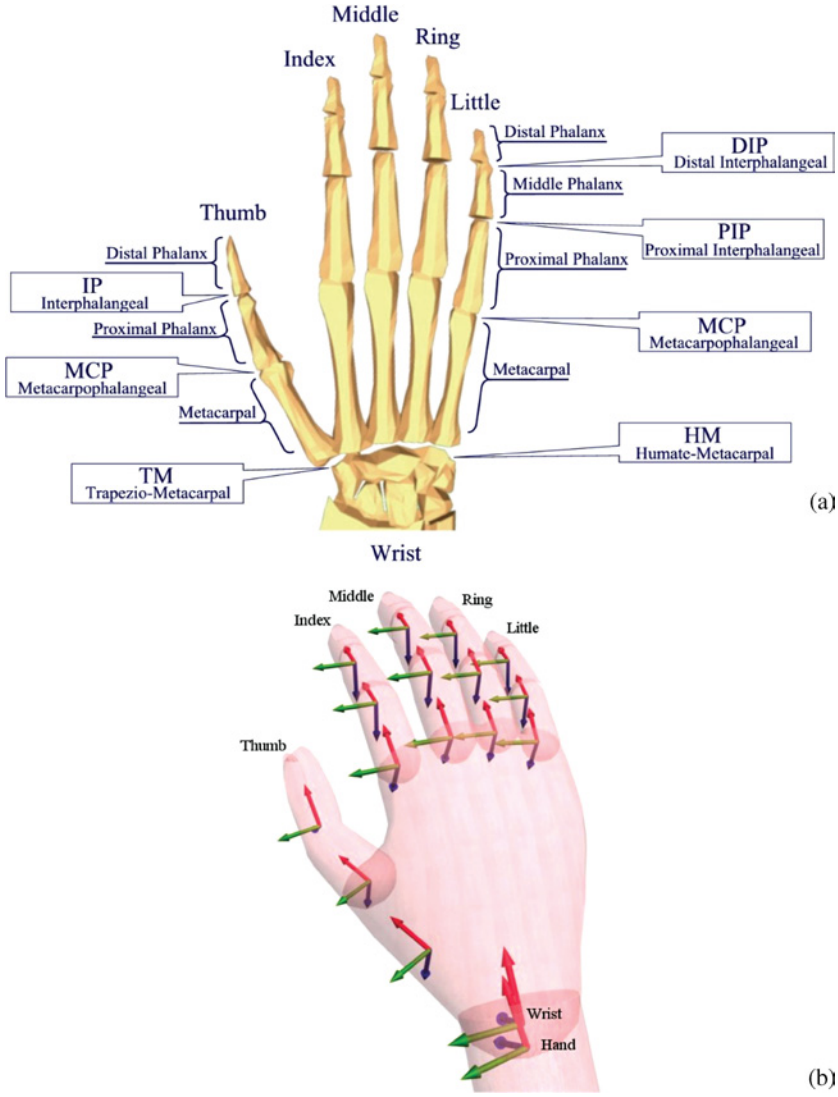

FIGURE 1. Anatomical details of the hand skeleton (a) and local coordinate systems of the hand skeleton model (b). The thumb is characterized by three articulations (interphalangeal—IP, metacarpophalangeal—MCP and trapeziometacarpal—TM joints). The other fingers are identified by three articulations (distal interphalangea—DIP, proximal interphalangeal—PIP, metacarpophalangeal MCP joints). The wrist was given two functional DoFs. The TM joint of the thumb was characterized by two DoFs (flexion/extension and adduction/abduction) as well as the MCP joints of the other fingers. A single DoF (flexion/extension) was used to characterize the MCP and IP joints of the thumb as well as the PIP and DIP joints of the other fingers.

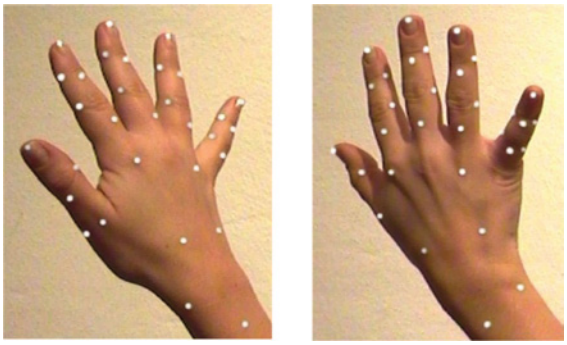

FIGURE 2. The marker protocol used to calibrate the hand model. Three markers were placed on the wrist dorsum to determine the global orientation and position of the model. Four markers were attached on the hand dorsum to define the wrist coordinate system.

Equivalently, excluding the metacarpal bone of the thumb, the assumption of grouping the four metacarpal bones into a single segment constitutes a good compromise between complexity and accuracy of the representation [see Fig. 1(b)]. In particular, the motions of the four metacarpal bones, which produce the deformation of the dorsum, are difficult to disaggregate from each other.

The dorsum was characterized by two functional DoFs, namely the flexion–extension and the abduction–adduction. Both distal and middle phalange joints were characterized by one functional DoF for flexion-extension. The proximal phalange joints were represented by two functional DoFs. The skeletal structure of the thumb was described by three joints: the metacarpal joint and the joints of the two phalanges were characterized by two DoFs and 1 DoF each, respectively. To compute the parameters of the proposed model, i.e., the relative position of the joint centers and the direction of the rotation axes, a configuration of 42 markers was utilized (Fig. 2(a) and 2(b)). Three markers, located approximately at the ulna styloid process, radius styloid process and wrist upper surface, were used to determine the wrist coordinate frame and the global position and orientation of the model. Four markers were placed on the hand torso to determine the dorsum coordinate frame and the direction of wrist flexion axis. The thumb was fit with seven markers, three at the metacarpal segment, three at the proximal phalanx and one at the distal phalanx. Equivalently, seven markers were used for the other fingers: three markers at the proximal phalanx, three markers at the middle phalanx, and one marker at the distal phalanx.

From movements involving the articulated motion of each anatomical segment, the 3D markers coordinates were computed in every frame of the sequence and used to calibrate the kinematic model.

Estimation of the Center and Axis of Rotation

The problem of calibrating the described model in terms of relative orientation and position of the coordinate system of the kinematic chain from 3D marker trajectories reconstructed in the motion sequence can be reformulated as the task of computing the temporal average of CoRs and AoRs. From mechanics, we know that pure planar rotational and 3D rotational motions determine an axis and a center of rotation, respectively. Assume that a cluster of markers performs a pure rotational motion around a center $\mathbf{c}$ or a rotation axis $\mathbf{a}$ in specific coordinate system. Rigid sphere fitting assumes that during the motion the relative position among the markers of the cluster does not vary.[26] The algorithm proposed by Gamage and Lasenby[12] extends the concept of sphere fitting by taking into account that during motion the markers are free to undergo different amounts of rotation among each other. Considering a rotation around the rotation center $\mathbf{c}$ of a cluster with M markers during N time steps, the cost function to minimize is represented by

$$f = \sum_{i}^{M} \sum_{j}^{N} \left[(\mathbf{p}_{i,j} - \mathbf{c}) \cdot (\mathbf{p}_{i,j} - \mathbf{c})^T - R_i^2 \right]^2 \qquad (1)$$

where $\mathbf{p}_{i,j}$ and R_i are the position of the ith marker at jth frame and the radius of the sphere defined by marker $\mathbf{p}_{i,j}$ around $\mathbf{c}$, respectively. Equivalently, for the rotation axis $\mathbf{a}$, the following equation is to be minimized:

$$f = \sum_{i}^{M} \sum_{j}^{N} [(\mathbf{p}_{i,j} - \mathbf{m}_i) \cdot \mathbf{a}]^2 \qquad (2)$$

where $\mathbf{m}_i$ is the perpendicular projection of $\mathbf{p}_{i,j}$ on $\mathbf{a}$ (Fig. 3). It was demonstrated that the minimization of Eq. (2) implies the computation of both the application point and the direction of the axis.[12]

The minimization of cost functions (1) and (2) were shown to be very sensitive to random noise in case of small ranges of motion (RoM). This can be even more important for the hand where intrinsic constraints of joints limit the segment mobility. In addition, marker motion artifacts in radial direction with respect to the rotation center or perpendicular to the axis direction were proved to introduce relevant bias in the estimation of both center and axis of rotation. In this case, even a wide range of motion does not guarantee accuracy.

To improve the accuracy of the estimation we proposed a new iterative algorithm based on single-membered evolutionary optimization, namely (1, λ)-ES evolution strategy method (ESM) with covariance matrix adaptation.[7] From a single element in the search domain (three coordinates of the rotation center), λ elements are generated by mutation, driven by previous selection results. After selecting the best element based on its fitness with respect to the cost function, the covariance matrix $\mathbf{C}^{(k)}$ at iteration step k, which determines the mutation function $\mathbf{M}^{(k)}$, is updated in such a way to generate offspring elements moving with increasing probability towards the optimal solution. The principle of adaptation is very similar to the discounted reward adopted

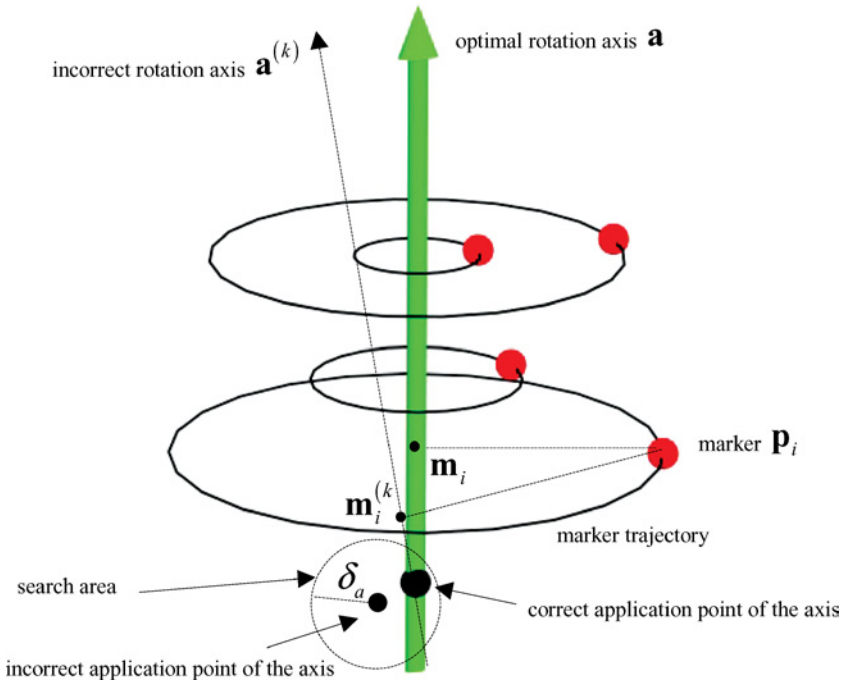

FIGURE 3. Determination of the rotation axis: application point and direction.

by reinforcement learning paradigm in machine learning.[15] Such a paradigm ensures that only mutation steps moving in the same direction, and chosen repeatedly, will be reinforced over time.[14] Given the best evolutionary path $\mathbf{S}^{(k)}$ obtained from selection process (innovation), the covariance matrix $\mathbf{C}^{(k+1)}$ at the next time step will be updated as

$$\mathbf{C}^{(k+1)} = (1-\alpha)\mathbf{C}^{(k)} + \alpha\mathbf{S}^{(k+1)} \tag{3}$$

where α is a scalar parameter utilized to weight the influence of the innovation $\mathbf{S}^{(k)}$ with respect to the past search history stored in $\mathbf{C}^{(k)}$ (see Cerveri *et al.*[7] for a detailed explanation of the role of the parameters and their setup values).

The cost function to be minimized is defined in such a way to express the dispersions of the distances of each marker $\mathbf{p}_{i,j}$ from the rotation center of the corresponding body segment along the whole motion sequence. The optimal rotation center is assumed to be the point with respect to which the root mean-squared error is minimal according to the following criterion:

$$f = \sum_{i}^{M}\sum_{j}^{N}\left(||p_{i,j} - c^{(k)}|| - \bar{R}_i^{(k)}\right) \tag{4}$$

where $\bar{R}_i^{(k)}$ is the average value of the distribution of distances at iteration step k, over the whole motion sequence, for the ith marker from the corresponding rotation center $\mathbf{c}^{(k)}$. The rotation center computed by Gamage and Lasenby algorithm [Eq. (1)] was used as the initialization of the evolutionary optimization procedure ($\mathbf{c}^{(0)}$). The optimization procedure stops when the solution is stable within a predefined threshold (Fig. 4).

For the estimation of the AoR, an equivalent evolutionary optimization was used to compute the application point and the direction of the axis. In order to increase stability and convergence speed, the axis estimation problem was split into two following steps, each having a search domain of three dimensions. Equation (2) was used to yield an initialization of both application point and direction of the

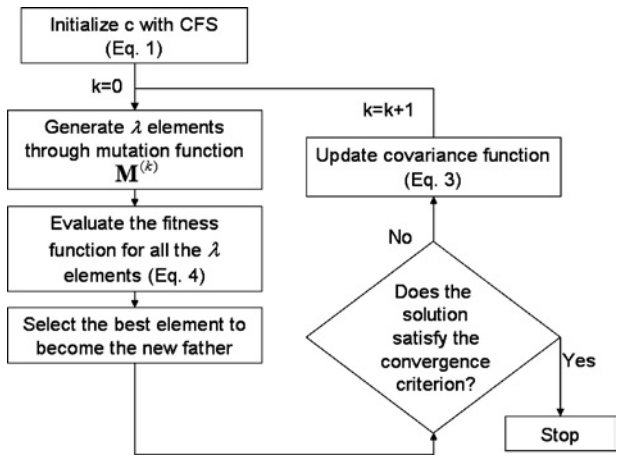

FIGURE 4. The chart of the optimization procedure to compute the rotation center. Substantially, the same chart can represent the procedure to determine the axis of rotation. $\lambda = 25$ elements were used in the evolutionary process. The parameter α, utilized to weight the influence of the innovation $\mathbf{S}^{(k)}$ with respect to the past search history stored in $\mathbf{C}^{(k)}$ [Eq. (3)], was setup to 0.25.

axis. In the first step, the application point of the axis was computed using a cost function equivalent to Eq. (4) with the additional constraint expressed as

$$\sqrt{\left(x - x_a^{(k)}\right)^2 + \left(y - y_a^{(k)}\right)^2 + \left(z - z_a^{(k)}\right)^2} < \delta_a \quad (5)$$

which represents the definition of a spherical search area of radius δ_a around the application point (x_a, y_a, z_a) computed by Eq. (2) (see Fig. 4). This constraint guaranteed a faster convergence to optimal solution.

In the second step, the direction of the axis was computed by iteratively minimizing the following cost function:

$$f = \sum_i^M \beta d_i^{(k)} \left(\sum_j^N \left(\mathbf{p}_{i,j} - \mathbf{m}_i^{(k)} \right) \cdot \mathbf{a}^{(k)} \right)^2 \quad (6)$$

where the influence of each marker was weighted proportionally to its averaged distance $d_i^{(k)}$ from the axis according to a parameter $\beta < 1$. This allowed increasing the role of the markers most distant from the axis and smoothing out the effect of noise on the closest markers as to improve the estimation accuracy.

The appealing characteristic of the evolutionary approach with respect to gradient-based optimization consists of the intrinsic ability to rapidly move away from local minima of the cost function[2] and converge towards the global optimum. Actually, the random-based mutation function produces most of the new elements nearby the actual best with few of them generated far away. The probability of falling into local minima clearly decreases as the number of elements λ increases.[7] Through a set of experiments on simulated data, involving the testing of numbers of elements ranging from 5 to 50 (step on was 5), we found that 25 elements were sufficient to skip local minima and approximate with great reliability the optimal solution in any condition.

Kinematic Chain Computation

The controlled hand movements were conceived to activate all the functional degrees of freedom of the hand skeleton. Note however that a generic articulated motion of the hand implies nonpure rotational movements of the markers attached at the hand dorsum and fingers. To attain pure rotations, the motions must be hierarchically decoupled from proximal to distal coordinate systems, i.e the direct kinematic of the chain must be solved. Starting from the wrist and proceeding to the coordinate system of distal phalanx joints, allows obtaining pure rotation motion in the local coordinate systems.

In the following, we will refer to functional coordinate system (FCS) and technical coordinate system (TCS) to indicate a coordinate system having or not functional meaning, respectively. The initial step of the procedure implied the computation of the TCS of the hand, used to represent the global orientation and position with respect to an external coordinate system. The location of the hand TCS was chosen as the mid point of the segment joining the two markers on the processes of the ulna and radius. The orthonormal basis of the coordinate system was found by applying the Graham Schmidt orthogonalization implemented through singular value decomposition.[24] For the construction of the FCS of the wrist, the 3D coordinates of the four markers on the surface of the hand dorsum were expressed in the technical coordinate system of the hand (namely the hand TCS). In this last coordinate system, the motion of such markers is a pure rotation with respect an unknown CoR (to be computed) that will be the location of the wrist FCS. The flexion/extension axis of the wrist was determined using pure flexion/extension motion patterns of the dorsum. The MCP CoRs of the fingers were computed by using pure rotational motion of the markers on the corresponding proximal phalanges obtained by computing a TCS from the four markers on the dorsum by Graham Schmidt orthogonalization and referring the marker coordinates to the TCS. The flexion/extension axes of the proximal interphalangeal (PIP) and distal interphalangeal (DIP) joints of the index were computed by referring the marker coordinates at the phalanges to the proximal and middle phalanx TCSs, respectively (Fig. 5).

To build the FCS of the wrist, expressed with respect to the hand TCS, we used the MCP CoR. The coordinates of the MCP CoR were first transformed from hand dorsum TCS into the hand TCS. Then the cross product between the segment, joining the MCP CoR of the finger index and the wrist CoR, and the wrist flexion axis provided the abduction/adduction direction of the wrist and by consequence the complete wrist FCS.

To compute the FCS of the MCP joint of the index finger we first transformed the MCP coordinates in the wrist FCS. Due to the intrinsic planar articulated movement of the fingers, the flexion/extension axis of the MCP joint was computed as the mean between the flexion/extension axes of the corresponding PIP and DIP joints whose coordinates were transformed in the wrist FCS. The CoR of PIP was computed as the intersection between the flexion axis of the PIP and perpendicular segment through the MCP CoR. Equivalently, the DIP CoR was computed as the intersection between the flexion axis of the DIP joint (DIP AoR) and the perpendicular segment through PIP CoR (Fig. 6).

Apart from the thumb, the same procedure was utilized to determine the FCS of the other finger joints. The CoR of the trapeziometacarpal (TM) joint of the thumb was computed by using the markers on the proximal phalanx whose coordinates was referred to the hand TCS. The flexion/extension axis of the TM joint was indirectly computed from the flexion/extension axis of the corresponding interphalangeal (IP) joint. The same axis direction was assigned to the flexion/extension axis of the MCP joint because of its very small RoM[11] preventing computation of the axis through marker trajectories.

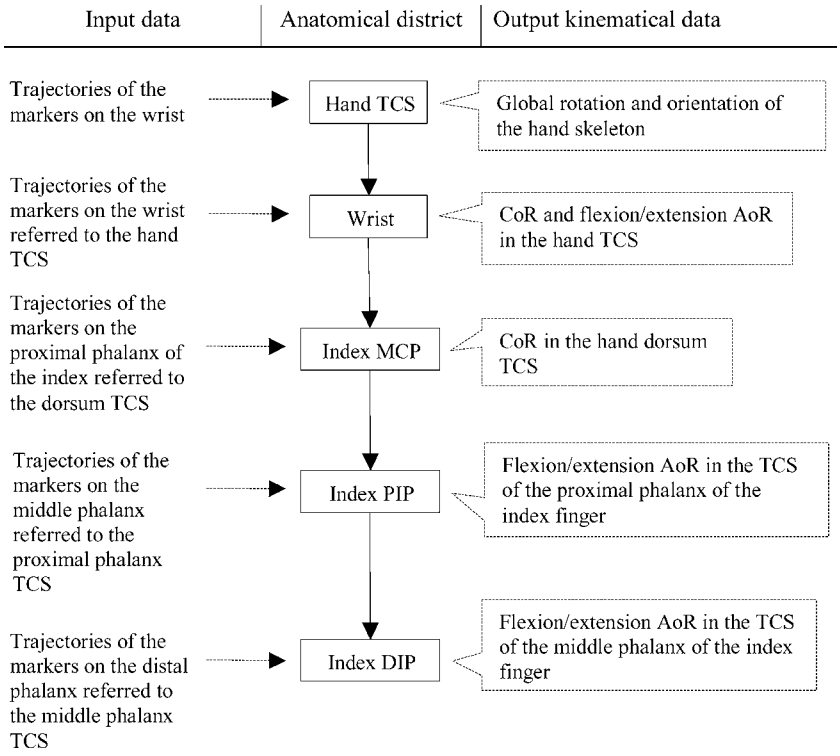

FIGURE 5. Hand skeleton calibration procedure. The detail of the determination of the CoR and AoR of the wrist and the phalanges and index finger. The functional coordinate systems (FCS) are determined by referring the CoR and AoR from technical coordinate system (TCS), into which they are computed, to proximal FCS.

EXPERIMENTAL VALIDATION

Simulated Motions

A virtual hand (typical adult male size) with a surface and skeleton model was designed within 3D StudioMax (Kinematics). Markers were placed on the external surface of the model according to the protocol of Fig. 2. Human-like articulated motions were generated through the key frame technique. Using such simulated motions, the proposed method (evolution strategy method: ESM) was compared with the Gamage and Lasenby method (closed-form solution: CFS) in terms of accuracy (the accuracy is the ability of a measurement to match the actual value of the quantity being measured) measured as the difference between the estimated variables (rotation centers and axis of rotation) and the nominal ones (ground truth).

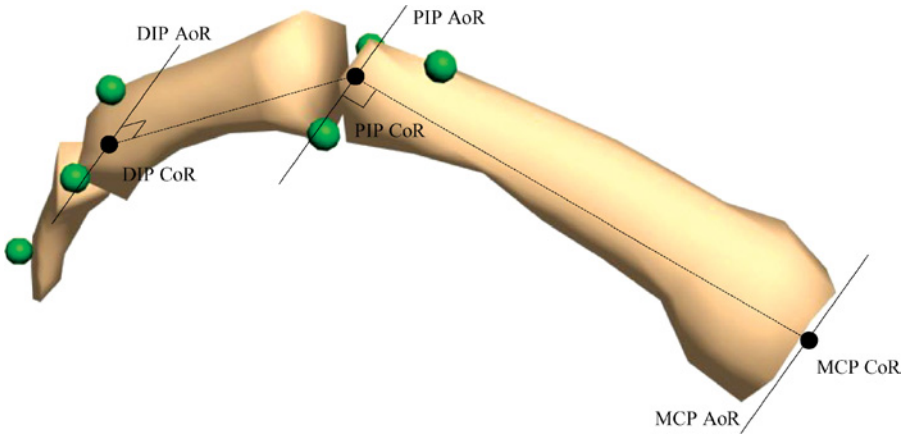

FIGURE 6. The PIP CoR is computed as the intersection between the PIP AoR and the perpendicular intersection of the straight line through the MCP. The DIP CoR is computed as the intersection between the DIP AoR and the perpendicular intersection of the straight line through the PIP CoR. The MCP AoR is determined as the averaged directions of PIP and DIP AoRs.

Rotation Center

The method was first validated on the computation of a single-rotation center by isolating the rotational component of motion of the three markers at the proximal phalanx of the index finger. Five motion patterns (time sampling frequency: 50 Hz; duration: 5 s) were generated with different amplitudes of motion (90°, 40°, 30°, 20°, and 10° of flexion/extension component with respect to the rest configuration). The RoM of the adduction/abduction component was setup to a fixed value of ±10° for all the five motion patterns.

The effects of measurement noise and systematic marker displacements were evaluated through two separate experiments. In the first session, uniformly distributed random noise, with four different amplitudes (0.1, 0.5, 1, and 2 mm) was used to perturb the 3D marker coordinates. The magnitude of such an error was chosen according to usual ranges of 3D accuracy provided by motion capture systems (Motion Analysis, Phoenix Technologies, Vicon, Oxford Metrix, Elite, BTS Engineering, Qualisys). Typically, into a calibrated working volume of about 50 cm × 50 cm × 50 cm, the 3D reconstruction accuracy is less than half a millimeter. Twenty-five random independent trials for each noise level were carried out and the accuracy was measured as the root mean squared error (Δ) of the distribution of the computed distances between estimated and nominal center.

As expected, the Δ increased as angular motion amplitude decreased (Fig. 7). This effect was particularly evident for CFS [RoM: 90°, rna (random noise amplitude): 1 mm, Δ: 1.27 mm; RoM: 10°, rna: 1 mm, Δ: 30.50 mm] whereas ESM showed a better behavior also for the smallest RoM (RoM: 90°, rna: 1 mm, Δ: 0.11 mm; RoM: 10°, rna: 1 mm, Δ: 3.22 mm). The reported results showed the sensitivity of CFS to random noise. The performance of CFS appeared to be satisfactory only for wide RoM, greater than 40°, but also in this case, ESM provided better accuracy. In particular, high accuracy was achieved by ESM with as little as 10° RoM (Fig. 7).

In the second session, a fixed uniform random noise (0.5-mm amplitude) was considered and a sinusoidal function in phase with the flexion of the index finger, with four different amplitudes (0.1, 0.5, 1, and 2 mm) was used to simulate the effects of marker displacements in radial direction caused by soft tissue artifacts. As discussed in,[12] this represents the more critical direction of artifact displacements. From the results, we found that the accuracy of the estimation by CFS was really affected by such artifacts (Fig. 8). CFS required large RoMs to provide adequate accuracy; however, at any RoM, the accuracy of CFS was less than half that of ESM for all artifact amplitudes. In contrast,

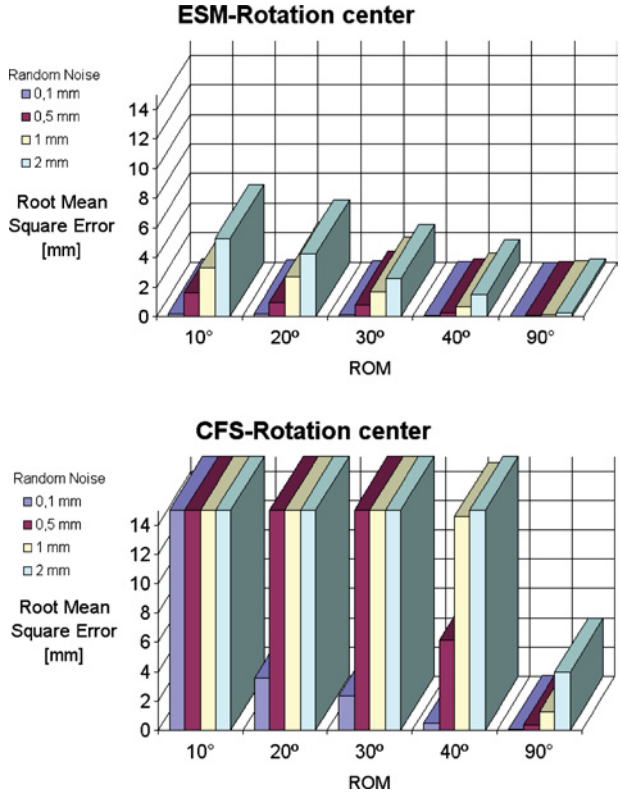

FIGURE 7. Error of the rotation center estimation as a function of the range of motion in correspondence of four increasing levels of random noise.

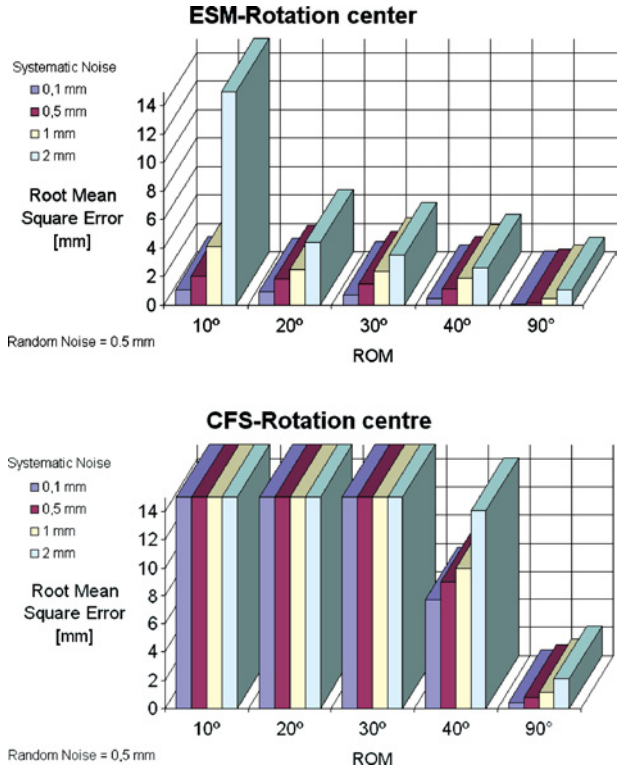

FIGURE 8. Error of the rotation center estimation as a function of the range of motion in correspondence of four increasing levels of systematic noise (random noise: 0.5 mm).

TABLE 1. Accuracy results of the estimated axis direction in function of the RoMs, random noise and motion artifacts.

		Range of motion									
		10°		20°		30°		40°		90°	
Random noise	Artifacts (mm)	ESM (°)	CFS (°)	ESM (°)	CFS (°)	ESM (°)	CFS (°)	ESM (°)	CFS (°)	ESM (°)	CFS (°)
0.5 mm	0.1	0.15	0.63	0.07	0.47	0.05	0.42	0.05	0.33	0.03	0.12
	0.5	0.31	1.18	0.16	1.08	0.13	0.77	0.07	0.89	0.06	0.24
	1	0.72	2.06	0.77	1.74	0.51	1.42	0.12	1.22	0.10	0.36
	2	1.77	3.37	1.62	2.89	0.67	2.53	0.27	2.04	0.22	0.86
1 mm	0.1	0.29	1.26	0.15	0.90	0.10	0.81	0.10	0.74	0.06	0.24
	0.5	0.62	2.95	0.31	2.15	0.25	1.94	0.15	1.78	0.11	0.48
	1	1.23	3.83	1.05	2.88	0.74	2.68	0.22	2.30	0.20	0.71
	2	2.23	5.03	1.98	3.97	0.84	3.55	0.34	2.77	0.28	1.41

ESM provided high accuracy for RoMs of at least 20°. For 10° RoM, only the smallest artifact amplitudes (0.1 and 0.5 mm) provided adequate accuracy (Δ: 1.10 mm; Δ: 2.04 mm). Higher artifacts amplitudes significantly affected the estimation (Δ: 4.09 mm; Δ: 15.18 mm).

Rotation Axis

In order to test the suitability of the method for the estimation of the rotation axis, a flexion/extension motion of the middle phalanx of the index finger was simulated. Five motion patterns (time sampling frequency: 50 Hz; duration: 5 s) were generated with different RoMs (90°, 40°, 30°, 20°, and 10°). The effects of motion artifacts, with four different amplitudes (0.1, 0.5, 1, and 2 mm), and two random noise levels (0.5–1 mm of standard deviation), on the accuracy of the estimation of the direction of the flexion axis were tested. Twenty-five random independent trials for each random noise level were carried out and the accuracy was measured as the root mean-squared error Δ of the distribution of the computed distances difference between the estimated axis direction and the nominal one (Table 1).

Results showed a good reliability of the ESM with accuracy better than 2.5° in the worst case [RoM: 10°, rna: 1 mm, sna (systematic noise amplitude): 2 mm]. For greater RoMs, ESM provided high accuracy (RoM: 20°, rna: 1 mm, sna: 2 mm, $\Delta = 1.98°$; RoM: 30°, rna: 1 mm, sna: 2 mm, $\Delta = 0.84°$). In contrast, CFS provided poor results also with greater RoMs (RoM: 20°, rna: 1 mm, sna: 2 mm, $\Delta = 3.97°$; RoM: 30°, rna: 1 mm, sna: 2 mm, $\Delta = 3.55°$). CFS was comparable to ESM only with the greatest RoM (90°), lower sna and lower rna.

Kinematic Chain

To test the method developed for estimating the complete hand skeleton model, 25 simulated motion sequences were generated imposing physiological-like ranges of motion (70°–90°). All the 3D marker coordinates were equally perturbed with a uniform random noise of 1-mm amplitude. Moreover, in order to simulate the hand dorsum deformation, we added a systematic noise (1-mm amplitude) to the coordinates of the four markers attached to it in phase with the little finger flexion. The perturbed direction was parallel to the dorsum surface to take into account the skin sliding over the skeleton. The estimation accuracy of each variable was computed as the RMS error of the distribution of the 25 standard deviations with respect to the corresponding nominal values. As expected, we first verified that motion artifacts caused a decrease of accuracy in the estimation of the wrist kinematics (Table 2). However, no relevant error propagation from proximal to distal joints was obtained.

Real Movements

The validation of the method on real hand motions was carried out across a set of 25 motion trials (duration: 15 s each) performed by a normal subject with the marker protocol defined in Fig. 3 (marker size: 3 mm). The articulated motions involved the action of all the functional DoFs with wide RoMs of the fingers and dorsum. The Elite system (Bioengineering Technology Systems, Milan, Italy) equipped with six cameras was used to acquire (sampling frequency: 100 Hz) and reconstruct 3D marker data. The system calibration accuracy was verified (0.25 mm) by measuring the RMS error of the distribution of the reconstructed distance between two rigidly linked markers, at known dis-

TABLE 2. Accuracy results (25 motion sequences with 1-mm measurement random noise) of the estimated hand skeleton with simulated motions.

		Rotation center (mm)		Flexion Axis (°)	
District	Joint	ESM	CFS	ESM	CFS
Hand	wrist	0.90	3.95	0.41	1.31
Thumb	TM	0.16	1.27	0.34	2.20
	MCP	0.14	1.38	0.83	1.75
	IP	0.21	1.04	0.92	1.90
Index finger	MCP	0.17	0.77	0.28	2.15
	PIP	0.70	1.49	1.10	2.12
	DIP	0.98	1.69	1.05	3.76
Middle finger	MCP	0.07	0.64	0.32	2.33
	PIP	0.70	1.48	1.12	2.49
	DIP	0.57	1.37	1.38	3.06

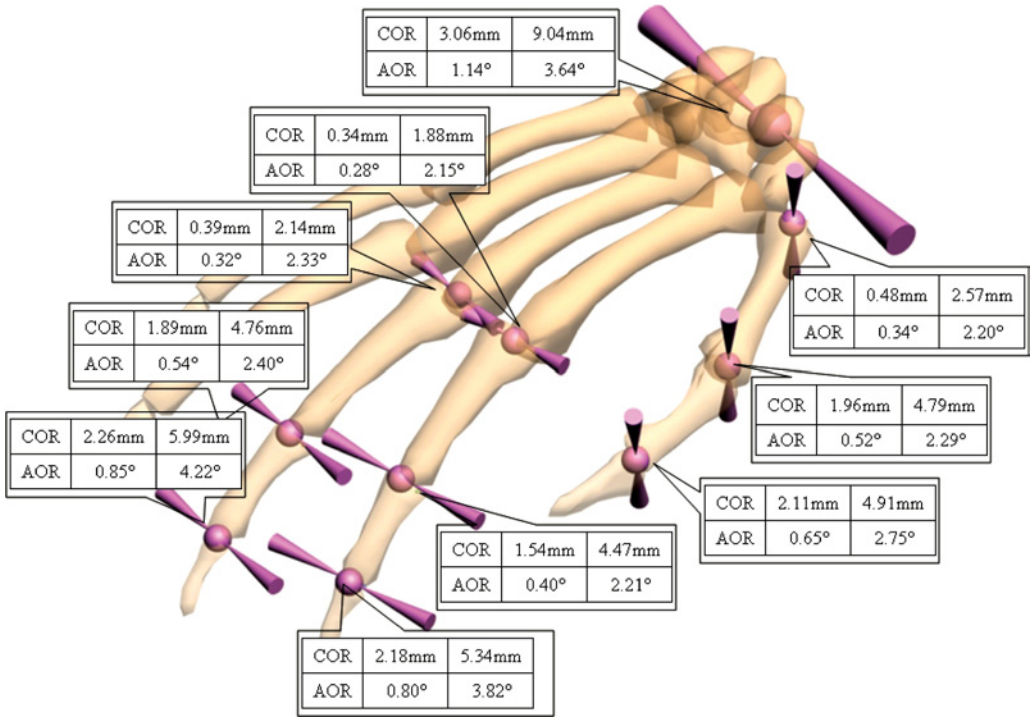

FIGURE 9. Results by ESM (left in captions) and CFS (right in captions) on real hand motion. The repeatability was measured in terms of CoR and AoR (flexion/extension) dispersion error computed as the standard deviation of the corresponding distributions over 25 motion trials. Without loss of generality, we reported the results for wrist, thumb, index, and middle fingers.

tance, acquired in several positions within the working volume (70 cm $\times$ 70 cm $\times$ 70 cm). For each motion trial, the kinematic chain was computed using marker trajectories subsampled by a factor of 5 in such a way to obtain some 3000 samples for each marker quite homogenously distributed along the ranges of motion. The performance of the estimation technique was measured in terms of repeatability (repeatability means yielding the same or compatible results in different experiments or statistical trials), expressed by the standard deviation σ of the distribution of the rotation center positions and rotation axis directions estimated from the 25 motion sequences (Fig. 9). Essentially, a true accuracy experiment using real data is extremely difficult to perform, requiring some invasive technique (bone pins, radiography, etc) applied simultaneously with video data.

Without loss of generality, the results for wrist, thumb, index, and middle fingers were reported. As results showed, CFS was unable to provide sufficient reliability for both CoRs and AoRs. Errors of several millimeters and some degrees were reported for CoR (wrist: 9.04 mm; index MCP: 1.88 mm; index PIP: 4.47 mm; index DIP 5.34 mm) and AoR (wrist: 3.64°; index PIP: 2.21°; index DIP 3.82°), respectively. In the light of results presented in Tables 1 and 2, the observed error range lead us to assert that the markers on the fingers and hand dorsum undergo not negligible motion artifacts, due to muscle inflation, and that CFS is not robust to such physiological systematic noise at all.

In contrast, ESM showed better reliability in the range of few millimeters and less than one degree for CoR and AoR, respectively. In particular, the accuracy of the estimation of the wrist CoR (3.06 mm) was less than that of the other joints (thumb TM: 0.48 mm, index MCP: 0.34 mm, middle MCP: 0.39 mm). This was motivated by considering that the four markers on the hand dorsum undergo some deformation during finger motion and, as proved in simulated experiments (Table 2), this disturbed the estimation. However, the amplitude of the reported error was reasonable. As regards the accuracy of the wrist flexion/extension AoR estimation, we reported the same previous accuracy decrease with respect the other joints. The obtained accuracy on the AoR was in the range of one degree. The greater dispersion of the DIP CoRs (index: 2.18 mm, middle: 2.26 mm) with respect to that of the corresponding PIP CoRs (index: 1.54 mm, middle: 1.89 mm) was attributed to the use of a single marker to determine the flexion/extension AoR of the DIP joint. In fact, the estimation error of the index PIP AoR (0.40°) was twice less than that of DIP (0.80°) AoR.

DISCUSSION AND CONCLUSIONS

The growing biomedical and physiological interest in studying hand motion *in vivo* has not led to concomitant investigations into the development of techniques to accurately measure finger kinematics. Undoubtedly, video-based surface measurements using markers in

correspondence to palpable bony landmarks have constituted a valuable source of data. Nevertheless, there is no consensus on a definitive approach and only few methods have been proposed. These techniques have not been extensively validated.[17,21,29] Recently, some researchers[30] begun to focus the attention on the attempt of developing robust and efficient techniques to estimate hand kinematics from surface markers. Accordingly, this paper proposed hand skeleton model and developed a set of methods that demonstrated a set of algorithms to compute the model kinematic variables from reconstructed motion of the markers with better performances than that obtained using classical techniques of nonrigid sphere fitting (CFS).[12] The developed methods (ESM) integrated an evolutionary optimization algorithm to enhance robustness, increase convergence properties and improve sensitivity to measurement noise.

For the hand skeletal model, an approximation of the metacarpal bones in the palm was made into a single kinematic joint and reduced the kinematic features of the thumb into three joints. We acknowledge that more accurate modeling would require the representation of each metacarpal segment with a proper joint. However, it appears quite difficult to apply a motion-based approach to determine their kinematic characteristics due to a very small RoM. Equivalently, while a more realistic modeling of the thumb could be obtained by splitting the TM joint into two joints, surface measurements would fail to correctly constraint the involved kinematics. In addition, large motion artifacts at the thumb base would prevent consistent kinematic estimation.

Extensive experiments on simulated motions showed that the estimation of single CoR and AoR by ESM is robust to random measurement noise even in case of very small RoMs (Fig. 7). CFS was insensitive to noise only for greater RoMs (90°). Experiments in presence of systematic noise (soft tissue artifacts) on the marker trajectories proved that ESM fails only with very small RoMs and higher noise amplitude (Fig. 8 and Table 1). In the case of greater artifacts, we found the estimation of the CoR more critical than that of AoR. However, for all tested conditions, ESM outperformed CFS. The computation of the whole hand kinematic model from simulated motions provided low propagation errors across following joints (Table 2). Results by ESM on real motions showed repeatability in the range of one millimeter, on the localization of the CoRs, and in the range of few tenths of degrees, on the axis directions (Fig. 9). These results demonstrated the reliability of the proposed method.

While the utilized marker placement scheme involved 42 markers, no tracking problems were experienced in the trajectory reconstruction because of slow calibration movements, the number of cameras, and small marker size (0.3 mm). In addition, the kinematic model estimation can be considered one-off procedure and the motion analysis of specific motion pattern can be attained with a reduced set of markers by removing the markers on the lateral finger surface. In this case, the calibrated skeleton model can be utilized within a model-based motion reconstruction framework as recently proposed in literature.[8]

ACKNOWLEDGMENT

This work was partially supported by BTS, Milano, Italy.

REFERENCES

[1]Alexander, E. J., and T. P. Andriacchi. Correcting for deformation in skin-based marker systems. *J. Biomech.* 34:355–361, 2001.

[2]Bäck, T., G. Rudolph, and H. P. Schwefel. Evolutionary programming and evolution strategies: Similarities and differences. In: Proceedings of the Second Annual Conference on Evolutionary Programming, edited by D. B. Fogel and W. Atmar. La Jolla, CA: Evolutionary Programming Society, 1993, pp. 11–22.

[3]Biggs, J., and K. Horch. A three-dimensional kinematic model of the human long finger and the muscles that actuate it. *Med. Eng. Phis.* 21:625–639, 1999.

[4]Brand, P. W., and A. M. Hollister. Clinical Biomechanics of the Hand, 3rd ed. St. Louis, MO: Mosby, 1999.

[5]Buchholz, B., and T. J. Armstrong. A kinematic model of the human hand to evaluate its prehensile capabilities. *J. Biomech.* 25:149–162, 1992.

[6]Cappozzo, A., F. Catani, A. Leardini, M. G. Benedetti, and U. Della Croce. Position and orientation in space of bones during movement: experimental artifacts. *Clin. Biomech.* 11:90–10, 1996.

[7]Cerveri, P., A. Pedotti, and N. A. Borghese. Combined evolution strategies for dynamic calibration of video-based movements measurement systems. *IEEE Trans. Evol. Comput.* 5:271–282, 2001.

[8]Cerveri, P., A. Pedotti, and G. Ferrigno. Model-based approach and extended Kalman filters for accurate human motion estimation. *Hum. Move. Sci.* 22:377–404, 2003.

[9]Coert, J. H., H. G. van Dijke, S. E. Hovius, C. J. Snijders, and M. F. Meek. Quantifying thumb rotation during circumduction utilizing a video technique. *J. Orthoped. Res.* 21:1151–1155, 2003.

[10]Chiu, H. Y., F. C. Su, S. T. Wang, and H. Y. Hsu. The motion analysis system and goniometry of the finger joints. *J. Hand Surg. B* 23:788–791, 1998

[11]Flanagan, J. R., and R. S. Johansson. Hand movements. *Encycloped. Hum. Brain* 2:399–414, 2002.

[12]Gamage, S. S. H. U., and J. Lasenby. New least square solutions for estimating the average center of rotation and axis of rotation. *J. Biomech.* 35:87–93, 2002.

[13]Halvorsen, K., M. Lesser, and A. Lundberg. A new method for estimating the axis of rotation and the center of rotation. *J. Biomech.* 32:1221–1227, 1999.

[14]Hansen, N., and A. Ostermeier. Completely derandomized self-adaptation in evolution strategies. *Evol. Comput.* 9:159–195, 2001.

[15]Kaelbing, L. P., M. L. Littman, and A. W. Moore. Reinforcement learning: A survey. *J. Artific. Intell. Res.* 4:237–285, 1996.

[16]Leijnse, J. N., C. J. Snijders, J. E. Bonte, J. M. Landsmeer, J. J. Kalker, J. C. Van der Meulen, G. J. Sonneveld, and S. E. Hovius. The hand of the musician: The kinematics of the bidigital finger

system with anatomical restrictions. *J. Biomech*. 26:1169–1179, 1993.
[17]Leijnse, J. N. and J. J. Kalkar. A two-dimensional kinematics modal of the lumbrical in the human finger. *J. Biomech*. 28:237–249, 1995.
[18]Lundberg, A. On the use of bone and skin markers in kinematics research. *Hum. Move. Sci*. 15:411–422, 1996.
[19]Marin, F., H. Mannel, L. Claes, and L. Dürselen. Accurate determination of a joint rotation center based on the minimal amplitude point method. *Comp. Aided Surg*. 8:30–42, 2003.
[20]Novak, K. E., L. E. Miller, and J. C. Houk Kinematic properties of rapid hand movements in a knob turning task. *Exp. Brain Res*. 132:419–433, 2000.
[21]Rash, G. S., P. P. Belliappa, M. P. Wachowiak, N. N. Somia, and A. Gupta. A demonstration of validity of 3-D video motion analysis method for measuring finger flexion and extension. *J. Biomech*. 32:1337–1341, 1999.
[22]Reinschmidt, C., A. J. van den Bogert, B. M. Nigg, A. Lundberg, and N. Murphy. Effect of skin movement on the analysis of skeletal knee joint motion during running. *J. Biomech*. 30:729–732, 1997.
[23]Pavlovic, V., R. Sharma, and T. S. Huang. Visual interpretation of hand gestures for human–computer interaction: A review. *IEEE Patt. Anal. Mach. Intell*. 19(7):677–695, 1997.
[24]Press, W. H., B. P. Flannery, S. A. Teukolsky, and W. T. Vetterling. Numerical Recipes in C. Cambridge, UK:Cambridge University Press, 1992.
[25]Santello, M., M. Flanders, and J. F. Soechting. Patterns of hand motion during grasping and the influence of sensory guidance. *J. Neurosci*. 22:1426–1435, 2002.
[26]Silaghi, M., R. Plaenkers, R. Boulic, P. Fua, and D. Thalmann. Local and global skeleton fitting techniques for optical motion capture. In: Modelling and Motion Capture Techniques for Virtual Environments, Lecture Notes in Artifcial Intelligence, No. 1537, edited by N. Magnenat-Thalmann and D. Thalmann. Berlin: Springer, 1998, pp. 26–40.
[27]Söderkvist, T., and P.-A. Wedin. Determining the movements of the skeleton using well-configured markers. *J. Biomech*. 12:1473–1477, 1993.
[28]Wu, W., M. J. Black, D. Mumford, Y. Gao, E. Bienenstock, and J. P. Pavlovic. Modeling and decoding motor cortical activity using a switching Kalman filter. *IEEE Trans. Biomed. Eng*. 51(6):933–942, 2004.
[29]Wu, Y., and T. S. Huang. Hand modeling, analysis and recognition, for vision-based human computer interaction. *IEEE Sign. Process. Mag*. 1053-5888/01/s10.00, 2001.
[30]Zhang, X., S. W. Lee, and P. Braido. Determining finger segmental centers of rotation in flexion-extension based on surface marker measurement. *J. Biomech*. 36:1097–1102, 2003.